Journal of Hydrology: Regional Studies 52 (2024) 101676

Contents lists available at ScienceDirect

Journal of Hydrology: Regional Studies

journal homepage: www.elsevier.com/locate/ejrh

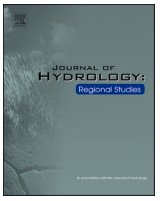

The effect of flood-mitigation reservoir configuration on peak-discharge reduction during preliminary design

Dina Pirone *, Luigi Cimorelli, Domenico Pianese

Department of Civil, Architectural and Environmental Engineering, University of Naples Federico II, Italy

ARTICLE INFO

Keywords:
Detention dams
Retention ponds
Flood regulation
Lamination effect
Flow peak reduction
Peak-discharge curves

ABSTRACT

Study region: The study considers synthetic river catchments representative of Mediterranean regions, with high impervious coverage and real rainfall time series.
Study focus: Stormwater studies often require rapid procedures to estimate which reservoir configuration reduces peak discharge to desired levels. Such estimates help identify and evaluate potential reservoir sites or assess the efficiency of existing ones. This paper provides simplified relationships to quantify the effects of the bottom outlet type and reservoir stage-storage curves on peak discharge reduction immediately downstream of a single reservoir.
New hydrological insight for the region: The proposed relationships fit the numerical results of detailed flood-routing simulations for 36 configurations. Results showed that the reduction effect could vary by 175% more, depending on the reservoir configuration. The proposed formulae allow a rapid evaluation and comparison of the reduction effect offered by different reservoir configurations without applying the standard reservoir-routing procedure, which should then refine and verify the design.

1. Introduction

Flood-mitigation reservoirs reduce peak discharge by retaining a portion of the flood volume until it can be gradually released. They are sustainable solutions that can help prevent flood damage and reduce the risk of downstream flooding and erosion. Indeed, their bottom outlets can allow the passage of the incoming sediment during floods and minimise the downstream impacts on the river environment (Brunner and Naveau, 2023; Sumi et al., 2011). Moreover, flood-mitigation reservoirs can enhance stormwater quality by promoting sedimentation, infiltration, and biological uptake (Nogherotto et al., 2022).

The design of a flood-mitigation reservoir requires the evaluation of several factors, ranging from site selection to technical features of the outlet structures and environmental characteristics. After the design has been established, the effect of a reservoir on peak discharge reduction is usually examined through hydrological and hydrodynamic simulations (Zhou, 2020). Comprehensive mathematical modelling and numerical methods are required to analyse reservoir systems. These yield detailed results at the expense of a considerable amount of information and high computational efforts (Cipollini et al., 2023; Del Giudice et al., 2014).

However, many stormwater studies often require a more rapid and straightforward procedure to estimate the detention storage volume needed to reduce flood discharge to desired levels (Abd-el-Kader et al., 2023; Ferrari et al., 2023). Such estimates help identify and evaluate potential sites for detention reservoirs. Indeed, it is possible for a reservoir to exacerbate the negative impact of flooding

* Corresponding author.
E-mail address: dina.pirone@unina.it (D. Pirone).

https://doi.org/10.1016/j.ejrh.2024.101676
Received 1 September 2023; Received in revised form 13 January 2024; Accepted 17 January 2024
Available online 25 January 2024
2214-5818/© 2024 The Author(s). Published by Elsevier B.V. This is an open access article under the CC BY license (http://creativecommons.org/licenses/by/4.0/).

or to have little to no effect on it (Tang et al., 2023; Wang et al., 2023). Thus, preliminary sizing can reduce the time and costs connected to the project and study. Moreover, rapid estimates can also be used to evaluate the efficiency of existing reservoirs in reducing flood peak discharge (Abd-el-Kader et al., 2023; Ravazzani et al., 2014). For example, after several years of reservoir operation, the peak reduction effect can change due to sedimentation processes, reclamation, or land-use changes. Therefore, its re-estimation is crucial for strategic risk management (Peng et al., 2006). For this reason, systematic reservoir storage surveys of a reservoir are periodically conducted to estimate the peak reduction effect.

Several approximate and simplified relationships for preliminary reservoir design are already available in the literature (Gioia, 2016; Sordo-Ward et al., 2013). Most of them express the ratio between the peak outflow, Q^*_{out}, and peak inflow, Q^*_{in}, as a function of the ratio between the flood retained by the reservoir, W^* , and the incoming volume, W_{in}, which hereafter are indicated as lamination ratio η and flood-storage ratio w, respectively (Eqs. 1 and 2).

$$\eta = \frac{Q^*_{out}}{Q^*_{in}} \tag{1}$$

$$w = \frac{W^*}{W_{in}} \tag{2}$$

Marone (1964) was one of the first who derived formulae of this type using geometric approximations for the inflow hydrographs, showing that the lamination ratio and flood-storage ratio are related by Eq. 3:

$$\eta = (1 - w)^{\xi} \tag{3}$$

where ξ varies according to the type of outlets. For overflow outlets, $\xi = 1$, whereas for bottom outlets, $\xi = 1.5$. However, these formulae did not consider the geometry of the reservoirs since they mainly assessed the impact of different types of outlets. Kessler and Diskin (1991) evaluated the relationships between the storage volume and the peak reduction ratio in two linear equations. They demonstrated that the inflow hydrograph shape did not influence the relationship between η and 1-w. Nevertheless, they only considered reservoirs with vertical walls. Along with previous authors, McEnroe (1993) derived approximate relationships from a reservoir-routing analysis, demonstrating that the peak-discharge ratios were determined primarily by the type of outlet and, to a lesser extent, by the shape factor of the inflow hydrograph. Hong et al. (2006) constructed different combinations of inflow and outflow hydrographs and provided equations to calculate the detention storage volume for each. However, they did not investigate the effect of the different storage configurations. Sordo-Ward et al. (2013) emphasised the general behaviour of the reduction effect and considered a wide range of basin area sizes, hydrologic loads, and reservoir and gate-controlled spillways. However, their results were conditioned to some assumptions, such as the initial reservoir water level being set to maximum and the gated spillway discharging the entire flow during the flood event.

The previous authors analysed and compared various aspects of peak reduction phenomena. However, their studies yield widely different estimates of the relationships for detention reservoir requirements. Indeed, the existing relationships are valid only for specific types and shapes of the inflow hydrographs. Moreover, these do not account for the considerable sensitivity of the peak discharge reduction to the geometry of the reservoir. Indeed, the size and shape of the reservoir, and thus the surrounding topography, affect the feasibility and cost-effectiveness of construction and the project's potential environmental and social impacts (Bellu et al., 2016). Thus, considerations about the geometry should be one of the first when dealing with flood mitigation purposes. Therefore, some vital and relevant aspects regarding the impact of geometry still need to be addressed.

This paper leads to new and simplified formulae for assessing the configuration impact of flood-mitigation reservoirs on peak discharge reduction. They represent a simplified approach that considers the features of a reservoir to estimate the peak discharge reduction. Indeed, the originality of this study solution lies in the fact that the impact of the geometry is assessed and quantified regardless of the actual shape of flow hydrographs. On the one hand, the proposed approach could allow a rapid evaluation of the potential reduction effect for reservoirs with a volume of up to 1 million m^3 and 36 geometry configurations. On the other hand, the regression formulae could estimate which configuration reduces the peak discharge to desired levels. The procedure is a sound basis for screening and ranking possible configurations and sites of reservoirs. Once a detention site has been selected and a preliminary design has been developed, the standard reservoir-routing procedure refines and verifies the design.

The remainder of the paper is organised as follows. First, Section 2 describes the traditional flood routing methodology required to design a flood mitigation reservoir, and thus, it illustrates the design parameters involved, such as the ones of the Stage-outflow and Stage-storage curves. Then, Section 2.2 presents the synthetic case study used for the numerical flood-routing simulations; thus, the realistic hydrographs are considered. Section 3 illustrates and organises the results of the numerical simulations in order to derive the simplified relationships. To prove the applicability and performance of the formulae under different rainfall patterns and basin parameters, Section 3.3 introduces two other synthetic case studies and evaluates the performance of the formulae. Section 4 analyses the obtained relationships, compares them to existing ones and suggests future developments. Finally, Section 5 draws conclusions.

2. Material and methods

2.1. Methodology

The expression reservoir routing denotes the propagation of an inflow hydrograph through a reservoir (Basha, 1995). It involves the

solution of a system of three equations: 1) the continuity equation, 2) the energy conservation equation in the form of an outlet discharge equation and 3) a relationship describing the configuration of the reservoir as a function of water depth in it (Fiorentini and Orlandini, 2013; Cimorelli et al., 2015).

1) Continuity equation (or mass conservation equation):

$$Q_{in}(t) - Q_{out}(t) = \frac{dW(t)}{dt} \tag{4}$$

where $Q_{in}(t)$ and $Q_{out}(t)$ are the inflow and outflow discharge, respectively, $W(t)$ is the volume of water in the reservoir, and t is the time (Fig. 1).

2) Energy conservation equation:

$$Q_{out} = ch^{m} \tag{5}$$

where Q_{out} is the outflow discharge, h is the water level in the reservoir, measured from an approximate datum, and c and m are constant values that vary according to the type and geometry of the outlet. For overflow outlets $m = 1.5$, and h is measured from the crest, whereas for submerged outlets $m = 0.5$ and h is measured from the centreline of the orifice o pipe.

3) Stage-storage relationship:

$$W = \alpha h^{\beta} \tag{6}$$

where α and β are constant values that vary according to the type and geometry of the reservoir. In particular, the exponent β ranges between 1 and 4.5, where 1 is associated with a prismatic geometry with surrounding vertical walls, and 4.5 is associated with a more complex morphology closed by more gentle lateral slopes (Manfreda et al., 2021). The stage-storage relationship can be determined for natural retention basins using bathymetric maps or by processing Digital Elevation Models (DEM), and Eq. 6 can fit such functions. Several challenges may arise during the process, especially according to the accuracy and resolution of the DEM data, that can significantly impact the quality of the stage-storage relationships. However, many studies suggest how to describe stage-storage relationships where detailed bathymetry surveys are unavailable or sparse. For example, Nilsson et al. (2008) proposed an analytical approach using simple geometric data from geographic information system coverages or field studies.

The governing storage equations (Eqs. 4–6) are valid when the water surface is horizontal and the outflow is unaffected by tailwater. When combined, they give a nonlinear first-order ordinary differential equation whose solution requires numerical methods such as the method of finite differences. The system can be solved once the inflow time series and the parameters of Eqs. 5 and 6 are defined. Thus, the outflow hydrograph and the peak outflow Q^*_{out} are provided (Fig. 2). For each reservoir routing simulation, the ratio between peak outflow Q^*_{out} and peak inflow Q^*_{in} defines the lamination ratio η. In the same way, the ratio between the maximum flood volume retained by the reservoir W* and the flood volume W determines the flood-storage ratio w.

2.2. Synthetic case study

The case study considers 36 configurations: six geometries of the reservoirs and six of the outlet structures. First, an ideal river basin with a linear and time-invariant hydrologic response is considered (**2.1.1**). Then, the outlet structures are defined (**2.1.2**). Finally, the reservoir configurations, and thus their geometries, are set up (**2.1.3**).

2.2.1. Basin configuration and inflow time series

The study considers an ideal basin with a linear and time-invariant hydrologic response (Table 1). The hydrographs derive from the Instantaneous Unit Hydrograph (IUH) theory, which requires defining the rainfall time series and the response function or IUH (Eq. 7):

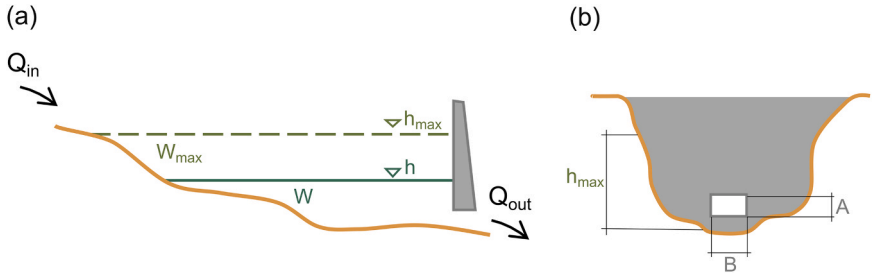

Fig. 1. Sketch of detention basin sections with a basin capacity of W_{max}. a) Longitudinal section, where Q_{in} is the inflow discharge, Q_{out} is the outflow discharge from gated bottom outlets, W is the storage, h is the water surface elevation, and h_{max} is the maximum water surface elevation; b) frontal section, where A is the height of the bottom outlet cross-section, and B is the width.

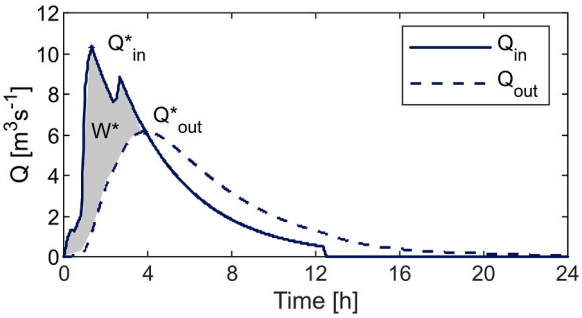

Fig. 2. Example of peak discharge reduction obtained via numerical simulation.

$$u(z) = \frac{1}{K} e^{-\frac{z}{K}} \quad \left[\frac{1}{T}\right] \tag{7}$$

where u(z) is the IUH ordinate at time z, z is the time, and K is the model's parameter. This application evaluated K according to VAPI Campania formulae (Rossi and Villani, 1995) (Table 1).

Once the rainfall time series is defined, the IUH theory provides an estimation of the discharges using the convolution integral (Eq. 8):

$$q_t = \int_0^t u(t-\tau) i_e(\tau) d\tau \tag{8}$$

where i_e is the net rainfall at the time t. Net rainfall is the fraction of precipitation that reaches the basin outlet as surface flow. It was obtained by multiplying the rainfall time series with a rational coefficient φ according to VaPi Campania formulae (Rossi and Villani, 1995) (Table 1). In what follows, for the sake of simplicity, we will refer to the net rainfall as rainfall. This study considers a rainfall time series of 19 years registered by a pluviographic station in Southern Italy (Fig. 3), with measurements every 10 min and 0.2 mm resolution. The continuous rainfall record is routed through the IUH, obtaining the corresponding streamflow time series (Fig. 3).

Finally, the hydrographs are extracted from the continuous streamflow record according to Peak-Over-Threshold (POT) and Minimum Inter-event Time (MIT) criteria (Pirone et al., 2023). These criteria allow selecting relevant and independent hydrographs from the continuous streamflow records (Paquet, 2019). On the one hand, the POT criterium allows focusing on significant flood events. Thus, only hydrographs with values higher than 0.5 m^3/s are considered. On the other hand, MIT criteria ensure that the selected hydrographs are independent. Indeed, one hydrograph must be separated from the previous or following by at least six hours. The procedure allows the selection of 1000 independent hydrographs.

2.2.2. *Outlet structures*

Six configurations of rectangular outlet cross-sections were considered (Fig. 4), with characteristics reported in Table 2. The outflow discharge curve derives from the physical modelling. For water levels lower than the height of the cross-section (A), a free surface behaviour characterises the flow through the bottom outlet with a critical state. As the water level in the reservoir increases (higher than A), the transition from free surface to submerged flow occurs – the choking effect. During this stage, the outflow decreases, and the behaviour follows the submerged outlet equation. However, due to the choking effect, the relationship between the outflow Q_{out} and the water level h becomes nonmonotonic. Thus, to avoid numerical problems, this study considers the flow constant during the choking effect (see Fiorentini and Orlandini, 2013 for further details). Thus, the flow is constant for water depths higher than A and lower than h_1. Finally, when the water level is higher than h_1, the flow follows the submerged flow equation. The value h_1 is computed as the intersection between the line Q_{out} constant and the submerged flow equation (Eq. 9). Indeed, according to the proper modelling, when the water level reaches the value of h_1, the flow increases again. Therefore, this modelling can be derived as follows:

$$Q_{out} = \begin{cases} Bh\sqrt{gh} & 0 \le h \le A \\ BA\sqrt{gA} & A < h \le h_1 \\ \mu\sigma\sqrt{2gh} & h > h_1 \end{cases} \tag{9}$$

where B [m] is the outlet width, h [m] is the water level in the reservoir, g [m^2/s] is the gravity acceleration, μ [-] is the coefficient of discharge of the bottom outlet, h_1 is height under which the outflow is constant, σ [m^2] is the area of the outlet cross-section.

Table 1
Main parameters of the river basin.

Area [km^2]	φ [-]	K [h]
100	0.70	3.00

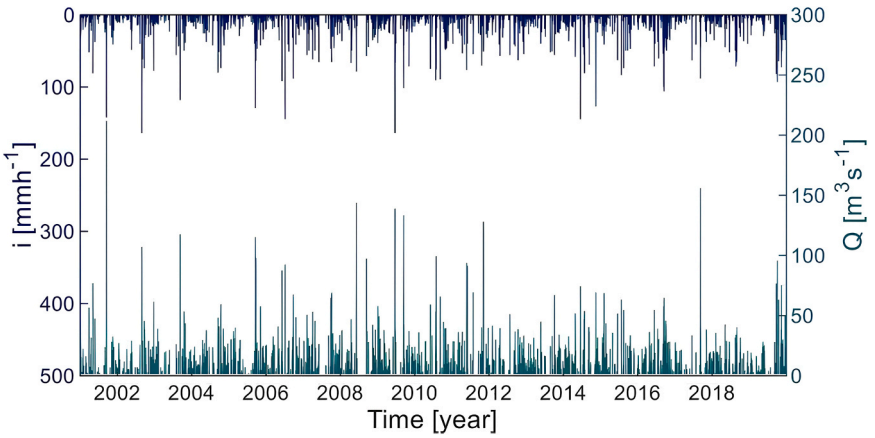

Fig. 3. Rainfall time series (i) and Inflow time series (Q).

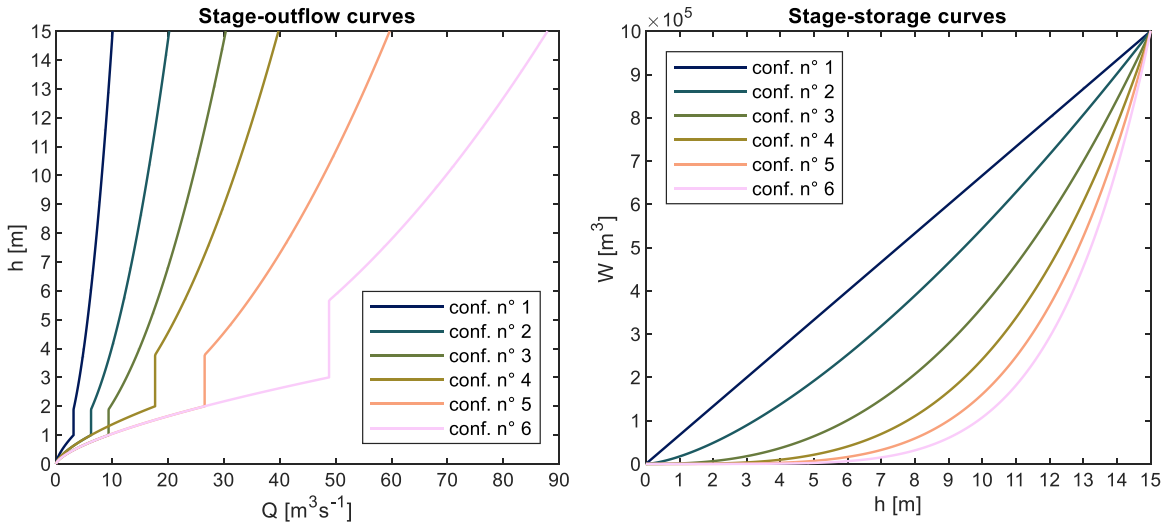

Fig. 4. left) Stage-outflow discharge (h–Q) curves obtained with Eq. 9 for six configurations (conf.) of outlet geometries (Table 2); right) Water level-storage curves (h–W) obtained from Eq. 6 with the parameters of Table 3.

Table 2
Parameters of the rectangular bottom outlet configurations. B is the width; A is the height of the cross-section.

Configuration n.	Width B [m]	Height A [m]
1	1	1
2	2	1
3	2	2
4	3	1
5	3	2
6	3	3

2.2.3. Geometry of the reservoir

Six reservoir configurations were considered (Table 3, Fig. 4). Each configuration, thus the geometry of the reservoir, is described through the stage-storage curves (Eq. 6). In this study, parameters α and β of Eq. 6 were chosen in order to provide a volume of 1 million of m^3 with regards to a water level of 15 m. Indeed, in Italy, these values define the limits between dams and large dams, with the latter requiring special attention both in the design and management stages.

2.3. Scenarios configuration

A total of 36 scenarios result from combining the six Outlet structure configurations with the six Geometry reservoir configurations (Table 4).

3. Results

3.1. Numerical results and simplified formulae

The lamination ratio η versus the flood-storage ratio 1 −w for all 1000 hydrographs and 36 reservoir configurations are graphically shown in Fig. 5, where each dot represents a numerical simulation result. In particular, results are grouped according to an n factor defined as the ratio between the exponent m of the discharge equation (Eq. 5) and the exponent β of the stage-storage curve (Eq. 6):

$$n = \frac{m}{\beta} \tag{10}$$

According to the chosen parameters, six values of n are obtained: 0.500, 0.333, 0.200, 0.143, 0.111, and 0.091.

For each of the six values of n, a cubic expression identifies the best regression curve (Eq. 11). Parameters a_0, b_0, c_0, and d_0 of Eq. 11 are obtained considering the boundary conditions, thus the passage through the points (0,0) and (1,1) of the plane (η, 1-w), and by minimising the sum of the Root Mean Square Error (RMSE) between the curve and each dot (Eq. 12).

$$\overline{\eta} = a_0(1-w)^3 + b_0(1-w)^2 + c_0(1-w) + d_0 \tag{11}$$

$$RMSE = \sqrt{\sum_{i=1}^{N} \frac{(\eta - \overline{\eta})^2}{N}}[-] \tag{12}$$

where η is the actual value, $\overline{\eta}$ is the estimated one, and N is the number of experimental dots, which are 36000 (1000 hydrographs for 36 configurations).

To highlight the dependence of the curves from n, the parameters a_0, b_0, c_0, and d_0 of Eq. 11 are linked to it. Thus, for every n, parameters a_0, b_0 and c_0 are plotted versus n (Fig. 6). Parameter d_0 is zero for every configuration due to the passage through the point (0,0) of the plane (η, 1-w).

According to Fig. 6, parameters a_0, b_0, c_0 vary linearly with n. Thus, the following preliminary relationship is derived:

$$\overline{\eta} = (-4.545 \bullet n + 1.052) \bullet (1-w)^3 + (4.322 \bullet n - 0.062) \bullet (1-w)^2 + (0.223 \bullet n + 0.011) \bullet (1-w) \tag{13}$$

where w is the ratio between the flood retained by the reservoir W* and the flood volume W_{in}. Finally, the proposed formulae are graphically shown for different values of n (Fig. 7).

For a particular value of the lamination ratio η, as n decreases, the flood-storage ratio w decreases (Fig. 7). Indeed, lower values of n correspond to higher values of the abscissa axis (1-w), thus to lower values of w. For example, to obtain the same lamination ratio η of 0.7, a reservoir with n = 0.500 requires a flood-storage ratio w of 0.297, while a reservoir with n = 0.333 requires a flood-storage ratio w of 0.210. Moreover, lower values of n correspond to higher values of β (Eq. 10). This means that reservoirs with more gentle lateral slopes (β > 1) reduce the peak discharge more than those with surrounding vertical walls (β = 1).

In contrast, for a particular value of the flood-storage ratio w, curves with higher values of n provide higher values of the lamination ratio η. For example, a flood-storage ratio w of 0.3 allows a peak lamination ratio of 0.40, 0.42, 0.44, 0.48, 0.58, 0.70 for a reservoir with n = 0.091, 0.111, 0.143, 0.200, 0.333, 0.500, respectively. Subsequentially, depending on the n, thus on the reservoir configuration, the lamination ratio η can vary from 0.40 to 0.70 (approximately 175% more).

3.2. Performance evaluation

The peak reduction ratios estimated with Eq. 13 were compared with the reference values obtained from the flood-routing simulations. The error metrics used were the RMSE (Eq. 12) and the absolute percentage error ε (Eq. 14) expressed as:

Table 3
Reservoir configuration. Parameters α and β derive from Eq. 6.

Configuration n.	α [m^2]	β[-]
1	66666.67	1.0
2	17213.26	1.5
3	1147.55	2.5
4	76.50	3.5
5	5.10	4.5
6	0.34	5.5

Table 4
Number of the scenario configurations obtained as a combination of outlet structures configuration (Table 2) and reservoir configuration (Table 3).

Outlet strucutres configuration	Geometry reservoir configuration					
	1	2	3	4	5	6
1	1	7	13	19	25	31
2	2	8	14	20	26	32
3	3	9	15	21	27	33
4	4	10	16	22	28	34
5	5	11	17	23	29	35
6	6	12	18	24	30	36

$$\varepsilon = \left|\frac{\eta - \overline{\eta}}{\eta}\right| \bullet 100[-] \tag{14}$$

Moreover, the predictive skill of the formulae was assessed with the Nash–Sutcliffe efficiency (NSE) (Eq. 15). This metric ranges between -Inf and 1, where "NSE = 1" corresponds to a perfect match.

$$\mathrm{NSE} = 1 - \frac{\sum_{i=1}^{N}(\eta - \overline{\eta})^2}{\sum_{i=1}^{N}(\eta - \mu_\eta)^2} \tag{15}$$

where μ_η is the mean value of the observed ones, and N is the number of simulations, which are 36,000 (1000 hydrographs for 36 configurations).

The average RMSE and percentage error ε between the actual values and those estimated with the proposed approach were 0.0662 and 12.84%, respectively (Fig. 8). Results were grouped according to the n factor, highlighting that, as n decreases, also the RMSE and percentage error ε decrease.

Finally, the NSE showed a value of 0.8519.

3.3. Additional results and validation of the formula

The derived formula was also applied to two other synthetic case studies. These further applications allowed testing the proposed formulae's applicability and performance under different rainfall patterns and basin parameters. In the first case, a different rainfall time series registered by another pluviographic station in Southern Italy was considered. The same rainfall time series of Fig. 3 was used in the second case but for another ideal river basin with parameters specified in Table 5, thus with an Area of 10 km^2.

In the first case, the average RMSE and percentage error ε between the actual values and those estimated with the proposed relationships were 0.0986 and 20.90%, respectively. Finally, the approach achieved a NSE of 0.7161.

In the second case, the average RMSE and percentage error ε between the actual values and those estimated with the proposed approach were 0.0714 and 17.07%, respectively (Fig. 8). Finally, the approach achieved a NSE of 0.8332.

Moreover, to prove that the formulae do not depend on the input hydrographs obtained from the chosen rainfall time series and the rainfall-runoff model, we considered six other synthetic hydrographs of different shapes, peak inflows and durations (Fig. 9, Table 6). In particular, we routed the six additional hydrographs according to the 36 configurations (Table 4) to obtain the actual values of the lamination ratio η and compare them to the lamination ratio suggested by the proposed relationships (Eq. 13). Results showed an average RMSE and percentage error ε of 0.068 and 9.52%, respectively.

4. Discussions

The study aimed to assess the configuration impact of flood-mitigation reservoirs on peak discharge reduction to provide simplified relationships that can be used during preliminary design.

4.1. Simplified formulae

The proposed relationships successfully fit the numerical results and correlate the reservoir geometry with the peak discharge reduction (Eq. 13). They describe the impact of different reservoir geometries on the peak discharge reduction thanks to a cubic expression through parameter n (Eq. 10). Experimental points in Fig. 5 tend to align along the shape of the stage-storage curves (Fig. 4, right). Indeed, as n decreases (thus, exponent β of the stage-storage curve increases), points tend to move away from the first sector bisector. This trend confirms that the geometry of the reservoir strongly influences the peak-reduction effect. For example, regarding the same flood-storage ratio and depending on parameter n, the relationships show that the lamination ratio η can vary up to 175% (Fig. 7).

Moreover, the performance evaluation showed that this simplified approach can successfully estimate the peak-reduction effect (Fig. 8). Indeed, the NSE is close to the optimal value of 1, and the mean RMSE and percentage error (ε) are low. Also, Fig. 8 shows that

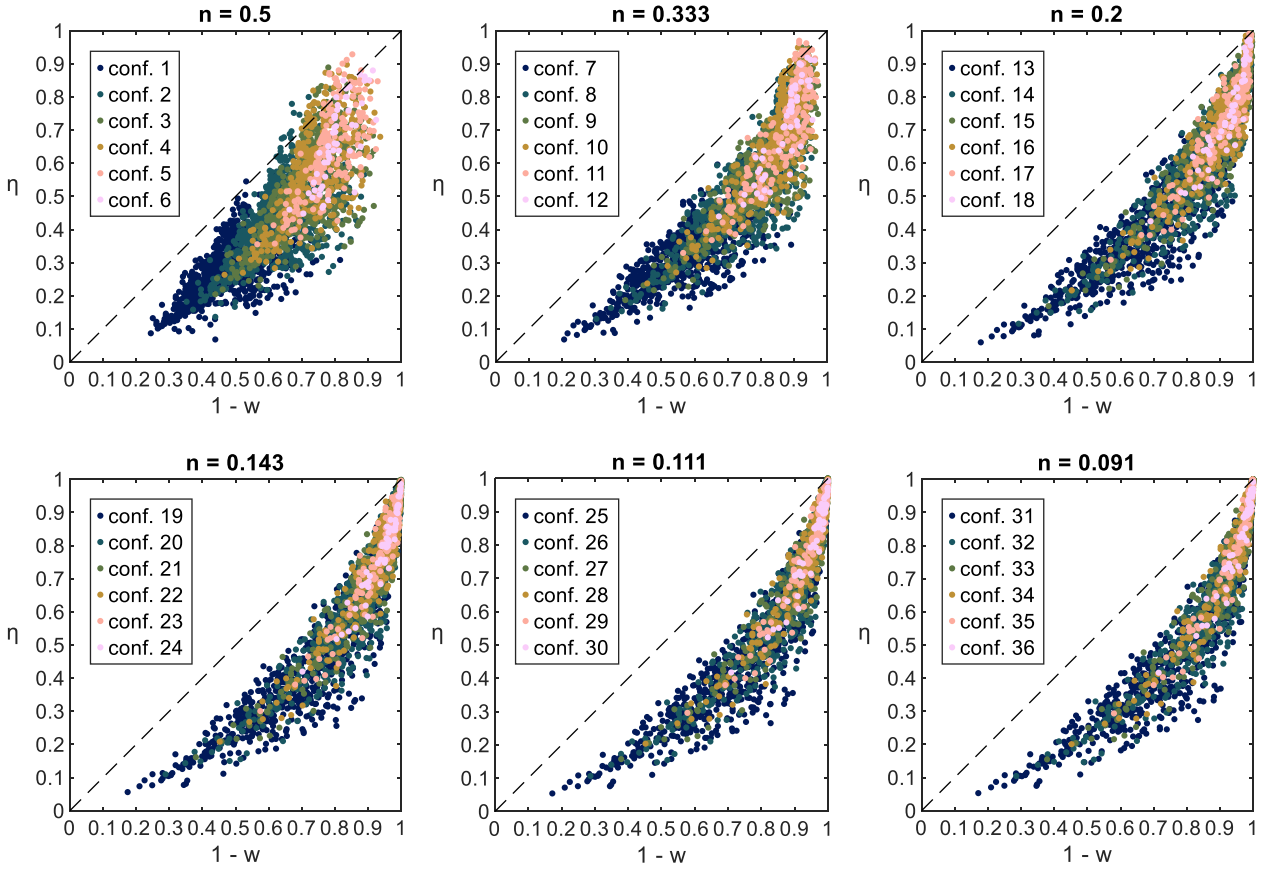

Fig. 5. Results of the lamination ratio η versus 1 - the flood-storage ratio (1-w) of the 1000 hydrographs for 36 combinations of reservoir configurations (Table 4), grouped into six graphs according to factor n (Eq. 9). Colours follow recommendations of scientifically derived colour maps (Crameri et al., 2020).

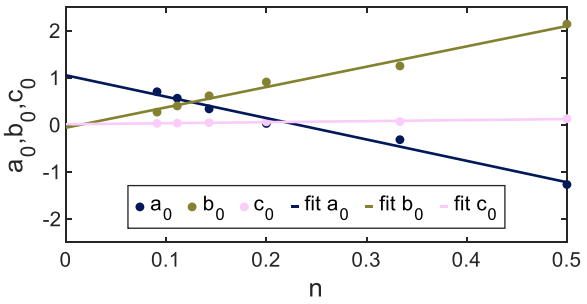

Fig. 6. Variation of parameters a_0, b_0, c_0 of Eq. 12 as a function of parameter n (Eq. 10). Dots represent values, while dashed lines represent the linear fittings.

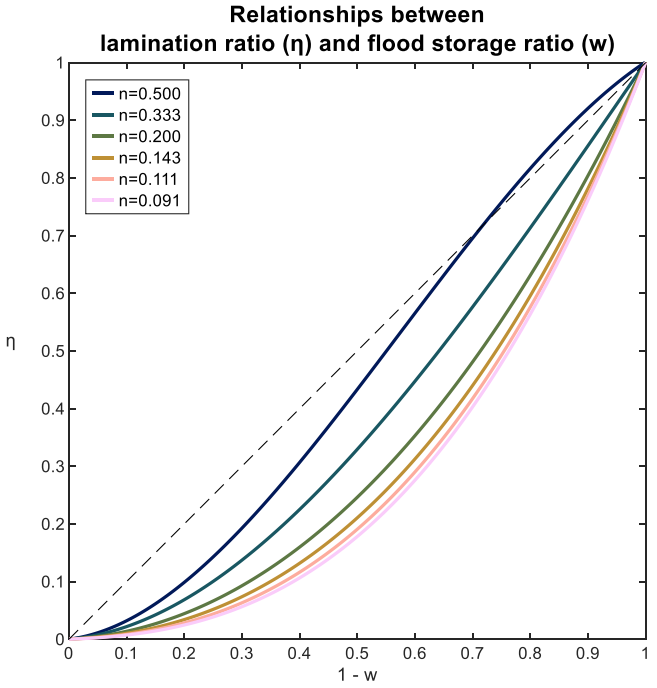

Fig. 7. Graphic representation of the relationship (Eq. 13) between the lamination ratio (η, Eq. 1) and 1 – the flood storage ratio (w, Eq. 2) for six values of parameter n (Eq. 10).

as n decreases, the error also decreases. This trend is coherent with the shape of the stage-storage curve. Indeed, when $n = 0.091$, $\beta = 5.5$, the volume variation of the reservoir is more gradual compared to the volume variation of $\beta = 1$ (on the stage-storage curve). In contrast, when $n = 0.5$, $\beta = 1$, thus the volume variation is sharper. Therefore, experimental points with higher values of n tend to be less dispersive than those characterised by higher values of n. As a result, as n decreases, the error between the actual value and the estimated one decreases.

Additional results from the other two case studies confirm the applicability of the proposed relationships to different hydrographs. Indeed, the additional case studies differ from the first in terms of rainfall time series and basin parameters, respectively. These supplementary applications enhance the formula's reliability, demonstrating its effectiveness in addressing varied hydrological analysis and water resource management scenarios across the study region.

The study also proved that the formulae are valid independently of the input hydrographs, thus independently of the chosen rainfall time series and the rainfall-runoff model. Indeed, six other synthetic hydrographs of different shapes, peak inflows and durations confirmed that the proposed relationships provide coherent results.

As a result, since the approach does not require the application of the classical reservoir routing equations, it yields rapid and valid results with low computational effort. Thus, a preliminary sizing with these formulae supports regional management needs and reduces the time and costs connected to the project and the study, ensuring that the overall project design is consistent with the objectives and requirements. This consistency is essential for the successful implementation and functionality of the infrastructure. Finally, preliminary sizing helps address concerns, garner support, and ensure that the reservoir design aligns with the needs of the

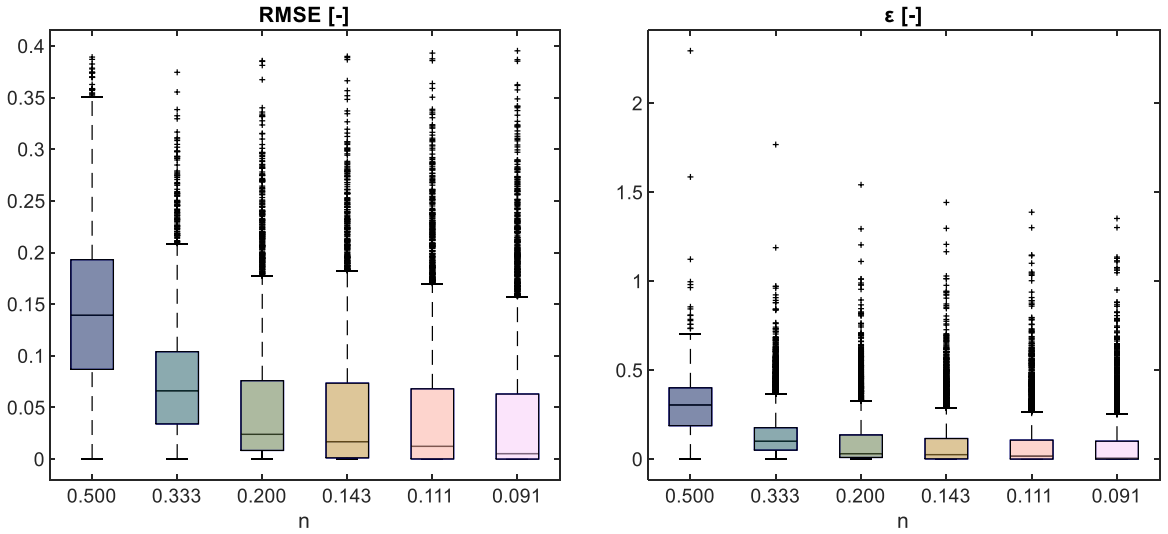

Fig. 8. Boxplots showing the Percentage error and RMSE between the observed data and those obtained with the proposed formula (Eq. 13).

Table 5
Main parameters of the river basin used to validate the formulae.

Area [km^2]	φ [-]	K [h]
10	0.70	3.00

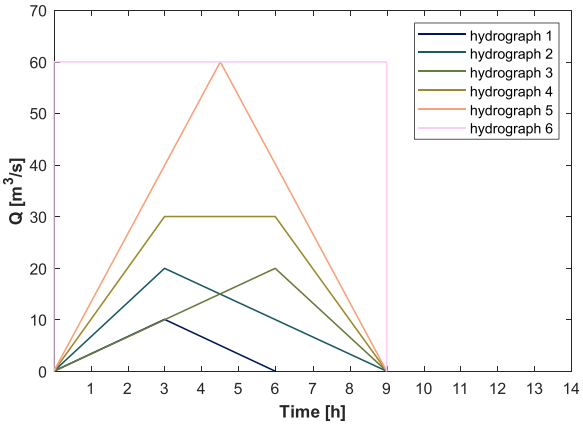

Fig. 9. Additional hydrographs considered to validate the formulae with characteristics reported in Table 6.

Table 6
Parameters of additional hydrographs considered to validate the formulae.

Hydrograph ID	Type of Shape	Q_{in}* [m^3/s]	W_{in} [m^3]
1	triangular	15.00	162,500
2	triangular	20.00	323,333
3	triangular	20.00	323,333
4	trapezoidal	30.00	646,667
5	triangular	60.00	970,000
6	rectangular	60.00	1,939,940

people in the region. By carefully planning the reservoir layout and associated infrastructure, it is possible to achieve economic efficiency.

4.2. Comparison with existing formulae

The relationships are also consistent with reference studies (Marone, 1964; McEnroe, 1993). In the plane (η, 1-w), values tend to spread under the first quadrant bisector, and the lamination ratio decreases as the slope of the reservoir walls decreases (Fig. 7). However, the previous formulae do not account for the reservoir configuration. For example, according to McEnroe (1993), a flood-storage ratio of 0.30 provides a lamination ratio of 0.80. In comparison, the relationships by Marone (1964) suggest a lamination ratio of 0.59 with regard to the same flood-storage ratio of 0.30. Such estimates broadly differ between them and the results from the simplified relationships obtained in this study. This difference is justified because most previous studies focused on the outlets' influence on peak discharge reduction. Thus, they did not highlight the influence of different geometries.

Indeed, the originality of this study solution lies in the fact that the impact of the geometry was assessed and quantified. The quantification is crucial because the available site strictly influences the geometry. Therefore, considerations about the geometry should be one of the first when dealing with flood mitigation purposes.

4.3. Future developments

This study considered reservoir configurations with bottom outlets. However, the definition of parameter n (Eq. 10) considers both the exponent of the discharge equation (Eq. 5) and the exponent of the stage-storage curve (Eq. 6). Therefore, this allows future studies to consider other outlet configurations. For example, future studies could consider scenarios with only overflow outlets or a combination of bottom and overflow outlets. These further configurations could provide helpful advances in the drought and flood risk field. Indeed, there is a recent attempt to consider interactions between these closely linked phenomena that are parts of the same hydrological cycle (Loon et al., 2021).

Finally, the relationship can be used for verification purposes. For example, it can estimate the effectiveness of existing reservoirs in reducing flood peak discharge. As a result, these estimates can define an order of priority for maintenance operations (Abd-el-Kader et al., 2023).

5. Conclusions

The proposed formula assesses and quantifies the geometry impact of detention reservoirs on peak discharge reduction. According to the performance indicators, the formulae successfully provide rapid and valid results with low computational effort. Indeed, the approach does not require the application of the classical reservoir routing equations. Therefore, the regression formulae represent a competitive approach for preliminary planning purposes for reservoirs with a volume of up to 1 million m^3 and 36 geometry configurations. They can be helpful for planners in the placement and sizing of detention reservoirs. Indeed, the formulae suggest which reservoir configuration allows reducing peak discharge reduction to desired levels. On the other hand, they also suggest the maximum reduction effect existing sites offer. As a result, when technical, time, or budget constraints do not permit a more precise method, the presented approach is a valid alternative to the standard reservoir routing equations, which should be later used to refine and verify the design.

CRediT authorship contribution statement

Pianese Domenico: Writing – review & editing, Writing – original draft, Supervision, Software, Resources, Methodology, Conceptualization. **Pirone Dina:** Writing – review & editing, Writing – original draft, Visualization, Validation, Software, Methodology, Formal analysis, Data curation, Conceptualization. **Cimorelli Luigi:** Writing – original draft, Supervision, Conceptualization.

Declaration of Competing Interest

The authors declare that they have no known competing financial interests or personal relationships that could have appeared to influence the work reported in this paper.

Data availability

The authors do not have permission to share data.

Appendix A. Notation

A1
Latin symbols.

a_0, b_0, c_0	Fitting parameters ofEq. 11.
A [m]	Height of the rectangular bottom outlet,Eq. 9,Table 2.
B [m]	Width of the rectangular bottom outlet,Eq. 9,Table 2.
c	Constant value of the energy conservation equation,Eq. 5.
h [m]	Variable water level in the reservoir.
K [h]	Constant of the IUH,Eq. 7.
m	Exponent of the energy conservation equation,Eq. 5.
n	Ratio between m and β,Eq. 10.
$Q_{in}(t)\left[m^3s^{-1}\right]$	Inflow hydrograph,Eq. 4.
$Q_{out}(t)\left[m^3s^{-1}\right]$	Outflow hydrograph,Eq. 4.
$Q^*_{in}\ \left[m^3s^{-1}\right]$	Peak inflow,Eq. 1.
$Q^*_{out}\left[m^3s^{-1}\right]$	Peak outflow,Eq. 1.
IUH	Instantaneous Unit Hydrograph,Eq. 7.
RMSE [-]	Root Mean Square Error,Eq. 12
$W\left[m^3\right]$	Variable volume of the reservoir.
$W_{in}\ \left[m^3\right]$	Volume of a flood event,Eq. 2.
$W^*\ \left[m^3\right]$	Maximum volume retained by the reservoir during a flood event,Eq. 2.
w	Ratio between W* and W_{in},Eq. 2.
t [s]	Time.
u	Instantaneous Unit Hydrograph,Eqs. 7 and 8.

A2
Greek symbols.

α $[m^2]$	Constant of stage-volume relationship,Eq. 6.
β	Exponent of stage-volume relationship,Eq. 6.
η	Ratio between the peak outflow Q^*_{out} and peak inflow Q^*_{in},Eq. 1.
φ [-]	Rational coefficient φ,Table 1.
ξ	Exponent ofEq. 1.
τ [s]	Time

References

Abd-el-Kader, M.M., El-Feky, A.M., Saber, M., AlHarbi, M.M., Alataway, A., Alfaisal, F.M., 2023. Designating appropriate areas for flood mitigation and rainwater harvesting in arid region using a GIS-based Multi-criteria decision analysis. Water Resour. Manag. 37, 1083–1108. https://doi.org/10.1007/s11269-022-03416-6.

Basha, H.A., 1995. Routing equations for detention reservoirs. J. Hydraul. Eng. 121, 885–888. https://doi.org/10.1061/(asce)0733-9429(1995)121:12(885).

Bellu, A., Sanches Fernandes, L.F., Cortes, R.M.V., Pacheco, F.A.L., 2016. A framework model for the dimensioning and allocation of a detention basin system: the case of a flood-prone mountainous watershed. J. Hydrol. 533, 567–580. https://doi.org/10.1016/j.jhydrol.2015.12.043.

Brunner, M.I., Naveau, P., 2023. Spatial variability in Alpine reservoir regulation: deriving reservoir operations from streamflow using generalized additive models. Hydrol. Earth Syst. Sci. 27, 673–687. https://doi.org/10.5194/hess-27-673-2023.

Cimorelli, L., Cozzolino, L., Della Morte, R., Pianese, D., Singh, V.P., 2015. A new frequency domain analytical solution of a cascade of diffusive channels for flood routing. Water Resour. Res. 51 (4), 2393–2411.

Cipollini, S., Volpi, E., Fiori, A., 2023. Toward a catchment-scale assessment of flood peak attenuation by multiple reservoirs. Water Resour. Res. 59, 1–20. https://doi.org/10.1029/2022WR032821.

Crameri, F., Shephard, G.E., Heron, P.J., 2020. The misuse of colour in science communication. Nat. Commun. 11, 5444. https://doi.org/10.1038/s41467-020-19160-7.

Del Giudice, G., Gargano, R., Rasulo, G., Siciliano, D., 2014. Preliminary estimate of detention basin efficiency at watershed scale. Water Resour. Manag. 28, 897–913. https://doi.org/10.1007/s11269-014-0518-1.

Ferrari, A., Vacondio, R., Mignosa, P., 2023. High-resolution 2D shallow water modelling of dam failure floods for emergency action plans. J. Hydrol. 618, 129192 https://doi.org/10.1016/j.jhydrol.2023.129192.

Fiorentini, M., Orlandini, S., 2013. Robust numerical solution of the reservoir routing equation. Adv. Water Resour. 59, 123–132. https://doi.org/10.1016/j.advwatres.2013.05.013.

Gioia, A., 2016. Reservoir routing on double-peak design flood. Water 8. https://doi.org/10.3390/w8120553.

Hong, Y.M., Yeh, N., Chen, J.Y., 2006. The simplified methods of evaluating detention storage volume for small catchment. Ecol. Eng. 26, 355–364. https://doi.org/10.1016/j.ecoleng.2005.12.006.

Kessler, A., Diskin, M.H., 1991. The efficiency function of detention reservoirs in urban drainage systems. Water Resour. Res. 27, 253–258. https://doi.org/10.1029/90WR02143.

Loon, A.Van, Ward, P.J., Ruiter, M.C.De, Mård, J., Schr, K., Veldkamp, T., Uexkull, N.Von, Wanders, N., Aghakouchak, A., Arnbjerg-nielsen, K., Capewell, L., Carmen, M., Day, R., Dewals, B., Di, G., Huning, L.S., Kreibich, H., Mazzoleni, M., Savelli, E., Teutschbein, C., Berg, H.Van Den, Heijden, A.Van Der, Vincken, J.M. R., Waterloo, M.J., Wens, M., 2021. The need to integrate flood and drought disaster risk reduction strategies. Water Sec. 11 https://doi.org/10.1016/j.wasec.2020.100070.

Manfreda, S., Miglino, D., Albertini, C., 2021. Impact of detention dams on the probability distribution of floods. Hydrol. Earth Syst. Sci. 25, 4231–4242. https://doi.org/10.5194/hess-25-4231-2021.

Marone, V., 1964. Calcolo di massima dell'effetto di laminazione di un serbatoio sulle piene. L'Energia Elettr. 46, 1–8.

McEnroe, B.M., 1993. Preliminary sizing'of detention reservoirs to reduce peak discharges. Search 118, 1540–1549.

Nilsson, K.A., Ross, M.A., Trout, K.E., 2008. Analytic method to derive wetland stage-storage relationships using GIS areas. J. Hydrol. Eng. 13, 278–282. https://doi.org/10.1061/(asce)1084-0699(2008)13:4(278).

Nogherotto, R., Fantini, A., Raffaele, F., Di Sante, F., Dottori, F., Coppola, E., Giorgi, F., 2022. A combined hydrological and hydraulic modelling approach for the flood hazard mapping of the Po river basin. J. Flood Risk Manag. 15, 1–17. https://doi.org/10.1111/jfr3.12755.

Peng, D., Guo, S., Liu, P., Liu, T., 2006. Reservoir storage curve estimation based on remote sensing data. J. Hydrol. Eng. 11, 165–172. https://doi.org/10.1061/(asce)1084-0699(2006)11:2(165).

Pirone, D., Cimorelli, L., Giudice, G., Del, Pianese, D., 2023. Short-term rainfall forecasting using cumulative precipitation fields from station data : a probabilistic machine learning approach. J. Hydrol. 617, 128949 https://doi.org/10.1016/j.jhydrol.2022.128949.

Ravazzani, G., Gianoli, P., Meucci, S., Mancini, M., 2014. Assessing downstream impacts of detention basins in urbanized river basins using a distributed hydrological model. Water Resour. Manag. 28, 1033–1044. https://doi.org/10.1007/s11269-014-0532-3.

Rossi, F., Villani, P., 1995. Flood evaluation in Campania Region (in Italian). GNDCI-CNR 1470 (Pubbl. N).

Sordo-Ward, A., Garrote, L., Bejarano, M.D., Castillo, L.G., 2013. Extreme flood abatement in large dams with gate-controlled spillways. J. Hydrol. 498, 113–123. https://doi.org/10.1016/j.jhydrol.2013.06.010.

Sumi, T., Kantoush, S.A., Shirai, A., 2011. Worldwide flood mitigation dams: operating and designing issues. Proc. Int. Symp. Urban Flood Risk Manag. 101–106.

Tang, X., Li, R., Wang, D., Jing, Z., Zhang, W., 2023. Reservoir flood regulation affects nutrient transport through altering water and sediment conditions. Water Res. 233, 119728 https://doi.org/10.1016/j.watres.2023.119728.

Wang, K., Pang, Y., Yi, Y., Yang, S., Wang, Y., He, C., Shi, Q., He, D., 2023. Response of dissolved organic matter chemistry to flood control of a large river reservoir during an extreme storm event. Water Res. 230, 119565 https://doi.org/10.1016/j.watres.2023.119565.

Zhou, Y., 2020. Exploring multidecadal changes in climate and reservoir storage for assessing nonstationarity in flood peaks and risks worldwide by an integrated frequency analysis approach. Water Res. 185, 116265 https://doi.org/10.1016/j.watres.2020.116265.